

Green Modulations in Energy-Constrained Wireless Sensor Networks

Jamshid Abouei[†], Konstantinos N. Plataniotis^{††}, and Subbarayan Pasupathy^{††}

[†] Department of Electrical Engineering, Yazd University, Yazd, Iran, Email: abouei@yazduni.ac.ir

^{††} The Edward S. Rogers Sr. Dept. of ECE, University of Toronto, Toronto, ON M5S 3G4, Canada

Emails: {kostas, pas}@comm.utoronto.ca

Abstract

Due to the unique characteristics of sensor devices, finding the energy-efficient modulation with a low-complexity implementation (referred to as *green modulation*) poses significant challenges in the physical layer design of Wireless Sensor Networks (WSNs). Toward this goal, we present an in-depth analysis on the energy efficiency of various modulation schemes using realistic models in the IEEE 802.15.4 standard to find the optimum distance-based scheme in a WSN over Rayleigh and Rician fading channels with path-loss. We describe a proactive system model according to a flexible duty-cycling mechanism utilized in practical sensor apparatus. The present analysis includes the effect of the channel bandwidth and the active mode duration on the energy consumption of popular modulation designs. Path-loss exponent and DC-DC converter efficiency are also taken into consideration. In considering the energy efficiency and complexity, it is demonstrated that among various sinusoidal carrier-based modulations, the optimized Non-Coherent M-ary Frequency Shift Keying (NC-MFSK) is the most energy-efficient scheme in sparse WSNs for each value of the path-loss exponent, where the optimization is performed over the modulation parameters. In addition, we show that the On-Off Keying (OOK) displays a significant energy saving as compared to the optimized NC-MFSK in dense WSNs with small values of path-loss exponent.

The work was supported in part by an Ontario Research Fund (ORF) project entitled “Self-Powered Sensor Networks”. The work of Jamshid Abouei was performed when he was with the Dept. of ECE, University of Toronto, Toronto, ON M5S 3G4, Canada. The material in this paper was presented in part to ICASSP’2010 conference, March 2010 [1].

Index Terms

Wireless sensor networks, energy efficiency, green modulation, M-ary FSK, Ultra-Wideband (UWB) modulation.

I. INTRODUCTION

Wireless Sensor Networks (WSNs) have been recognized as a collection of distributed nodes to support a broad range of applications, including monitoring, health-care and detection of environmental pollution. In such configuration, sensors are typically powered by limited-lifetime batteries which are hard to be replaced or recharged. On the other hand, since a large number of sensors are deployed over a region, the circuit energy consumption is comparable to the transmission energy due to the short distance between nodes. Thus, minimizing the total energy consumption in both circuits and signal transmission is a crucial task in designing a WSN [1], [2]. Central to this study is to find energy-efficient modulations in the physical layer of a WSN to prolong the sensor lifetime. For this purpose, energy-efficient modulations should be simple enough to be implemented by state-of-the-art low-power technologies, but still robust enough to provide the desired service. In addition, since sensor devices frequently switch from sleep mode to active mode, modulator circuits should have fast start-up times. We refer to these simple and low-energy consumption schemes as *green modulations*.

In recent years, several energy-efficient modulations have been studied in the physical layer of WSNs (e.g., [3], [4]). In [3] the authors compare the battery power efficiency of PPM and OOK based on the Bit Error Rate (BER) and the cutoff rate of a WSN over path-loss Additive White Gaussian Noise (AWGN) channels. Reference [4] investigates the energy efficiency of a centralized WSN with an adaptive MQAM scheme. However, adaptive approaches impose some additional system complexity due to the multi-level modulation formats plus the channel state information fed back from the sink node to the sensor node. Most of the pioneering work on energy-efficient modulations, including research in [3], has focused only on minimizing the average energy consumption per information bit, ignoring the effect of the bandwidth and transmission time duration. In a practical WSN, however, it is shown that minimizing the total energy consumption depends strongly on the active mode duration and the channel bandwidth [5].

In this paper, we present an in-depth analysis (supported by numerical results) of the energy efficiency of various modulation schemes considering the effect of the “*channel bandwidth*” and the “*active mode duration*” to find the distance-based green modulations in a proactive WSN. For this purpose, we describe the system model according to a flexible duty-cycling process utilized in practical sensor devices. This model distinguishes our approach from existing alternatives [3]. New analysis results for comparative evaluation of popular modulation designs are introduced according to the realistic parameters in the IEEE 802.15.4 standard [6]. We start the analysis based on a Rayleigh flat-fading channel with path-loss which is a feasible model in static WSNs [3]. Then, we evaluate numerically the energy efficiency of sinusoidal carrier-based modulations operating over the more general Rician model which includes a strong direct Line-Of-Sight (LOS) path. Path-loss exponent and DC-DC converter efficiency (in a non-ideal battery model) are also taken into consideration. It is demonstrated that among various sinusoidal carrier-based modulations, the optimized Non-Coherent M-ary Frequency Shift Keying (NC-MFSK) is the most energy-efficient scheme in sparse WSNs for each value of the path-loss exponent, where the optimization is performed over the modulation parameters. In addition, we show that the On-Off Keying (OOK) has significant energy saving as compared to the optimized NC-MFSK in dense WSNs with small values of path-loss exponent. NC-MFSK and OOK have the advantage of less complexity and cost in implementation than MQAM and Offset-QPSK used in the IEEE 802.15.4 protocol, and can be considered as green modulations in WSN applications.

The rest of the paper is organized as follows. In Section II, the proactive system model and assumptions are described. A comprehensive analysis of the energy efficiency for popular sinusoidal carrier-based and UWB modulations is presented in Sections III and V. Section IV provides some numerical evaluations using realistic models to confirm our analysis. Finally in Section VI, an overview of the results and conclusions are presented.

For convenience, we provide a list of key mathematical symbols used in this paper in Table I.

TABLE I

LIST OF NOTATIONS

B : Bandwidth	b : Number of bits per symbol
B_{eff} : Bandwidth efficiency	\mathcal{E}_t : Energy per symbol
d : Distance	\mathcal{E}_N : Total energy consumption for N -bit
M : Constellation size	h_i : Fading channel coefficient
P_s : Symbol error rate	\mathcal{L}_d : Channel gain factor in distance d
T_s : Symbol duration	N : Number of transmitted bits in active mode period
T_{ac} : Active mode period	\mathcal{P}_c : Total circuit power consumption
T_{tr} : Transient mode period	\mathcal{P}_t : RF transmit power consumption per symbol
η : Path-loss exponent	χ_e : Power transfer efficiency in DC-DC converter
$\Omega = \mathbb{E}[h_i ^2]$	γ_i : Instantaneous SNR
$\mathbb{E}[\cdot]$: Expectation operator	$\Pr\{\cdot\}$: Probability of the given event

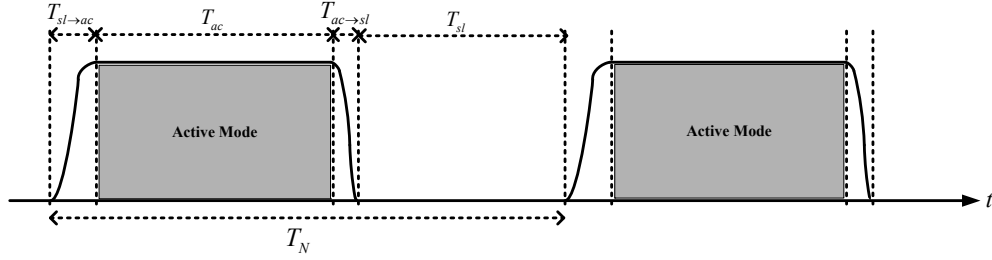


Fig. 1. A practical duty-cycling process in a proactive WSN.

II. SYSTEM MODEL AND ASSUMPTIONS

In this work, we consider a proactive wireless sensor system, in which a sensor node transmits an equal amount of data per time unit to a designated sink node. The sensor and sink nodes synchronize with one another and operate in a duty-cycling manner as depicted in Fig 1. During *active mode* period T_{ac} , the sensed analog signal is first digitized by an Analog-to-Digital Converter (ADC), and an N -bit binary message sequence $\mathbb{M}_N \triangleq \{a_i\}_{i=1}^N$ is generated, where N is assumed to be fixed. The bit stream is modulated using a pre-determined modulation scheme¹ and then transmitted to the sink node. Finally, the

¹Because the main goal of this work is to find the distance-based green modulations, and noting that the source/channel coding increase the complexity and the power consumption, in particular codes with iterative decoding process, the source/channel coding are not considered.

sensor node returns to the *sleep mode*, and all the circuits are powered off for the sleep mode duration T_{sl} . We denote T_{tr} as the *transient mode* duration consisting of the switching time from sleep mode to active mode (i.e., $T_{sl \rightarrow ac}$) plus the switching time from active mode to sleep mode (i.e., $T_{ac \rightarrow sl}$), where $T_{ac \rightarrow sl}$ is short enough to be negligible. Under the above considerations, the sensor/sink nodes have to process one entire N -bit message \mathbb{M}_N during $0 \leq T_{ac} \leq T_N - T_{sl} - T_{tr}$, where $T_N \triangleq T_{tr} + T_{ac} + T_{sl}$ is assumed to be fixed for each modulation, and $T_{tr} \approx T_{sl \rightarrow ac}$. Note that T_{ac} is an influential factor in choosing the energy-efficient modulation, since it directly affects the total energy consumption as we will show later.

We assume that both sensor and sink devices include a Direct Current to Direct Current (DC-DC) converter to generate a desired supply voltage from the embedded batteries. An DC-DC converter is specified by its *power transfer efficiency* denoted by $\chi_e < 1$. In addition, we assume a linear model for batteries with a small discharge current, meaning that the stored energy will be completely used or released. This model is reasonable for the proposed duty-cycling process, as the batteries which are discharged during active mode durations can recover their wasted capacities during sleep mode periods. Since sensor nodes in a typical WSN are densely deployed, the distance between nodes is normally short. Thus, the total circuit power consumption, defined by $\mathcal{P}_c \triangleq \mathcal{P}_{ct} + \mathcal{P}_{cr}$, is comparable to the RF transmit power consumption denoted by \mathcal{P}_t , where \mathcal{P}_{ct} and \mathcal{P}_{cr} represent the circuit power consumptions for the sensor and sink nodes, respectively. In considering the effect of the power transfer efficiency, the total energy consumption in the active mode period, denoted by \mathcal{E}_{ac} , is given by

$$\mathcal{E}_{ac} = \frac{\mathcal{P}_c + \mathcal{P}_t}{\chi_e} T_{ac}, \quad (1)$$

where T_{ac} is a function of N and the channel bandwidth as we will show in Section III. Also, it is shown in [7] that the power consumption during the sleep mode duration T_{sl} is much smaller than the power consumption in the active mode (due to the low sleep mode leakage current) to be negligible. As a result, the *energy efficiency*, referred to as the performance metric of the proposed WSN, can be measured by the total energy consumption in each period T_N corresponding to N -bit message \mathbb{M}_N as follows:

$$\mathcal{E}_N \approx \frac{1}{\chi_e} [(\mathcal{P}_c + \mathcal{P}_t)T_{ac} + \mathcal{P}_{tr}T_{tr}], \quad (2)$$

where $\frac{P_{tr}}{\chi_e} T_{tr}$ is the circuit energy consumption during the transient mode period. We use (2) to investigate and compare the energy efficiency of various modulation schemes in the subsequent sections.

Channel Model: It is shown that for short-range transmissions including the wireless sensor networking, the root mean square (rms) delay spread is in the range of ns [8] (and ps for UWB applications [9]) which is small compared to the symbol duration $T_s = 16 \mu s$ obtained from the bandwidth $B = \frac{1}{T_s} = 62.5$ KHz in the IEEE 802.15.4 standard [6, p. 49]. Thus, it is reasonable to expect a flat-fading channel model for WSNs. Under the above considerations, the channel model between the sensor and sink nodes is assumed to be Rayleigh flat-fading with path-loss. This assumption is used in many works in the literature (e.g., see [3] for WSNs). We denote the fading channel coefficient corresponding to symbol i as h_i , where the amplitude $|h_i|$ is Rayleigh distributed with the probability density function (pdf) $f_{|h_i|}(r) = \frac{2r}{\Omega} e^{-\frac{r^2}{\Omega}}$, $r \geq 0$, where $\Omega \triangleq \mathbb{E}[|h_i|^2]$ [10]. To model the path-loss of a link where the transmitter and receiver are separated by distance d , let denote \mathcal{P}_t and \mathcal{P}_r as the transmitted and the received signal powers, respectively. For a η^{th} -power path-loss channel, the channel gain factor is given by

$$\mathcal{L}_d \triangleq \frac{\mathcal{P}_t}{\mathcal{P}_r} = M_l d^\eta \mathcal{L}_1, \quad \text{with } \eta_{min} \leq \eta \leq \eta_{max}, \quad (3)$$

where M_l is the gain margin which accounts for the effects of hardware process variations and $\mathcal{L}_1 \triangleq \frac{(4\pi)^2}{\mathcal{G}_t \mathcal{G}_r \lambda^2}$ is the gain factor at $d = 1$ meter which is specified by the transmitter and receiver antenna gains \mathcal{G}_t and \mathcal{G}_r , and wavelength λ (e.g., [3], [5]). As a result, when both fading and path-loss are considered, the instantaneous channel coefficient becomes $G_i \triangleq \frac{h_i}{\sqrt{\mathcal{L}_d}}$. Denoting $x_i(t)$ as the transmitted signal with energy \mathcal{E}_t , the received signal at the sink node is given by $y_i(t) = G_i x_i(t) + z_i(t)$, where $z_i(t)$ is AWGN with two-sided power spectral density given by $\frac{N_0}{2}$. Thus, the instantaneous Signal-to-Noise Ratio (SNR) corresponding to an arbitrary symbol i can be computed as $\gamma_i = \frac{|G_i|^2 \mathcal{E}_t}{N_0}$. Under the assumption of a Rayleigh fading channel, γ_i is chi-square distributed with 2 degrees of freedom, with pdf $f_\gamma(\gamma_i) = \frac{1}{\bar{\gamma}} \exp\left(-\frac{\gamma_i}{\bar{\gamma}}\right)$, where $\bar{\gamma} \triangleq \mathbb{E}[|G_i|^2] \frac{\mathcal{E}_t}{N_0} = \frac{\Omega}{\mathcal{L}_d} \frac{\mathcal{E}_t}{N_0}$ denotes the average received SNR.

III. ENERGY EFFICIENCY ANALYSIS OF SINUSOIDAL CARRIER-BASED MODULATIONS

In this section, we analyze the energy and bandwidth efficiency of three popular sinusoidal carrier-based modulations, namely MFSK, MQAM and OQPSK, over a Rayleigh flat-fading channel with path-loss. FSK is used in many low-complexity and energy-constrained wireless systems and some IEEE standards (e.g., [11]), whereas MQAM is used in modem and digital video applications. Also, OQPSK is used in the IEEE 802.15.4 standard which is the industry standard for WSNs. In the sequel and for simplicity of the notation, we use the superscripts ‘FS’, ‘QA’ and ‘OQ’ for MFSK, MQAM and OQPSK, respectively.

M-ary FSK: An M-ary FSK modulator with $M = 2^b$ orthogonal carriers benefits from the advantage of using the Direct Digital Modulation (DDM) approach, meaning that it does not need the mixer and the Digital to Analog Converter (DAC). This property makes MFSK has a faster start-up time than the other modulation schemes. Let denote $\Delta f = \frac{1}{\zeta T_s^{FS}}$ as the minimum carrier separation with the symbol duration T_s^{FS} , where $\zeta = 2$ for coherent and $\zeta = 1$ for non-coherent FSK [12, p. 114]. In this case, the channel bandwidth is obtained as $B \approx M \times \Delta f$, where B is assumed to be fixed for all sinusoidal carrier-based modulations. Denoting B_{eff}^{FS} as the *bandwidth efficiency* of MFSK defined as the ratio of data rate $R^{FS} = \frac{b}{T_s^{FS}}$ (b/s) to the channel bandwidth, we have

$$B_{eff}^{FS} \triangleq \frac{R^{FS}}{B} = \frac{\zeta \log_2 M}{M}, \quad \text{b/s/Hz.} \quad (4)$$

It can be seen that using a small constellation size M avoid losing more bandwidth efficiency in MFSK. To address the effect of increasing M on the energy efficiency, we first derive the relationship between M and the active mode duration T_{ac}^{FS} . Since, we have b bits during each symbol period T_s^{FS} , we can write

$$T_{ac}^{FS} = \frac{N}{b} T_s^{FS} = \frac{MN}{\zeta B \log_2 M}. \quad (5)$$

Recalling that B and N are fixed, an increase in M results in an increase in T_{ac}^{FS} . However, the maximum value of T_{ac}^{FS} is bounded by $T_N - T_{tr}^{FS}$ as illustrated in Fig. 1. Thus, $M_{max} \triangleq 2^{b_{max}}$ in MFSK is calculated by the following non-linear equation:

$$\frac{M_{max}}{\log_2 M_{max}} = \frac{\zeta B}{N} (T_N - T_{tr}^{FS}). \quad (6)$$

At the receiver side, the received MFSK signal can be detected coherently to provide an optimum performance. However, the MFSK coherent detection requires the receiver to obtain a precise frequency and carrier phase reference for each of the transmitted orthogonal carriers. For large M , this would increase the complexity of the detector which makes a coherent MFSK receiver very difficult to implement. Thus, most practical MFSK receivers use non-coherent detectors². To analyze the energy efficiency of a NC-MFSK, we first derive \mathcal{E}_t^{FS} , the transmit energy per symbol, in terms of a given average Symbol Error Rate (SER) denoted by P_s . It is shown in [14, Lemma 2] that the average SER of a NC-MFSK is upper bounded by

$$P_s = 1 - \left(1 - \frac{1}{2 + \bar{\gamma}^{FS}}\right)^{M-1}, \quad (7)$$

where $\bar{\gamma}^{FS} = \frac{\Omega}{\mathcal{L}_d} \frac{\mathcal{E}_t^{FS}}{N_0}$. As a result, the transmit energy consumption per symbol is obtained from the above P_s as

$$\mathcal{E}_t^{FS} \triangleq \mathcal{P}_t^{FS} T_s^{FS} = \left[\left(1 - (1 - P_s)^{\frac{1}{M-1}}\right)^{-1} - 2 \right] \frac{\mathcal{L}_d N_0}{\Omega}. \quad (8)$$

In considering the effect of the DC-DC converter and using (5), the output energy consumption of transmitting N -bit during T_{ac}^{FS} is computed as

$$\frac{\mathcal{P}_t^{FS}}{\chi_e} T_{ac}^{FS} = \frac{T_{ac}^{FS}}{T_s^{FS}} \frac{\mathcal{E}_t^{FS}}{\chi_e} = \left[\left(1 - (1 - P_s)^{\frac{1}{M-1}}\right)^{-1} - 2 \right] \frac{\mathcal{L}_d N_0}{\chi_e \Omega} \frac{N}{\log_2 M}. \quad (9)$$

On the other hand, the total circuit energy consumption of the sensor/sink devices during T_{ac}^{FS} is obtained from $\frac{\mathcal{P}_{ct}^{FS} + \mathcal{P}_{cr}^{FS}}{\chi_e} T_{ac}^{FS}$. For the sensor node with the MFSK modulator, we denote the power consumption of frequency synthesizer, filters and power amplifier as \mathcal{P}_{Sy}^{FS} , \mathcal{P}_{Filt}^{FS} and \mathcal{P}_{Amp}^{FS} , respectively. In this case,

$$\mathcal{P}_{ct}^{FS} = \mathcal{P}_{Sy}^{FS} + \mathcal{P}_{Filt}^{FS} + \mathcal{P}_{Amp}^{FS}. \quad (10)$$

It is shown that the relationship between \mathcal{P}_{Amp}^{FS} and the transmission power of an MFSK signal is $\mathcal{P}_{Amp}^{FS} = \alpha^{FS} \mathcal{P}_t^{FS}$, where α^{FS} is determined based on the type of the power amplifier. For instance for a class B power amplifier, $\alpha^{FS} = 0.33$ [5]. For the circuit power consumption of the sink node, we use the fact that the optimum NC-MFSK demodulator consists of a bank of M matched filters, each followed

²For the purpose of comparison, the energy efficiency of a *coherent* MFSK is fully analyzed in Appendix I in [13].

by an envelope detector [15]. In addition, we assume that the sink node uses a Low-Noise Amplifier (LNA) which is generally placed at the front-end of a RF receiver circuit, an Intermediate-Frequency Amplifier (IFA), and an ADC, regardless of type of deployed modulation. Thus, denoting \mathcal{P}_{LNA}^{FS} , \mathcal{P}_{Filtr}^{FS} , \mathcal{P}_{ED}^{FS} , \mathcal{P}_{IFA}^{FS} and \mathcal{P}_{ADC}^{FS} as the power consumption of LNA, filters, envelope detector, IF amplifier and ADC, respectively, the circuit power consumption of the sink node is obtained as

$$\mathcal{P}_{cr}^{FS} = \mathcal{P}_{LNA}^{FS} + M \times (\mathcal{P}_{Filtr}^{FS} + \mathcal{P}_{ED}^{FS}) + \mathcal{P}_{IFA}^{FS} + \mathcal{P}_{ADC}^{FS}. \quad (11)$$

Moreover, it is shown that the power consumption during the transient mode period T_{tr}^{FS} is governed by the frequency synthesizer in both sensor/sink nodes [5]. Thus, the energy consumption during T_{tr}^{FS} is obtained as $\frac{\mathcal{P}_{tr}^{FS}}{\chi_e} T_{tr}^{FS} = 2 \frac{\mathcal{P}_{Sy}^{FS}}{\chi_e} T_{tr}^{FS}$ [8]. Substituting (5) and (9) in (2), the total energy consumption of a NC-MFSK scheme for transmitting N -bit in each period T_N and for a given P_s is obtained as

$$\begin{aligned} \mathcal{E}_N^{FS} = & (1 + \alpha^{FS}) \left(\left[1 - (1 - P_s)^{\frac{1}{M-1}} \right]^{-1} - 2 \right) \frac{\mathcal{L}_d N_0}{\chi_e \Omega} \frac{N}{\log_2 M} + \\ & \frac{1}{\chi_e} \left[(\mathcal{P}_c^{FS} - \mathcal{P}_{Amp}^{FS}) \frac{MN}{B \log_2 M} + 2 \mathcal{P}_{Sy}^{FS} T_{tr}^{FS} \right], \end{aligned} \quad (12)$$

with the fact that $\mathcal{L}_d = M_l d^\eta \mathcal{L}_1$. Thus, the optimization goal is to determine the optimum constellation size M , such that the objective function \mathcal{E}_N^{FS} can be minimized, i.e.,

$$\begin{aligned} \hat{M} = \arg \min_M \mathcal{E}_N^{FS} \\ \text{subject to } \begin{cases} 2 \leq M \leq M_{max} \\ \eta_{min} \leq \eta \leq \eta_{max} \\ d > 0, \end{cases} \end{aligned} \quad (13)$$

where M_{max} derived from (6). To solve this optimization problem, we prove that (12) is a monotonically increasing function of M for every value of d and η . It is seen that the second term in (12) is a monotonically increasing function of M . Also, from the first term in (12), we have

$$\left(\left[1 - (1 - P_s)^{\frac{1}{M-1}} \right]^{-1} - 2 \right) \frac{1}{\log_2 M} = \left(\left[1 - e^{\frac{1}{M-1} \ln(1-P_s)} \right]^{-1} - 2 \right) \frac{1}{\log_2 M} \quad (14)$$

$$\stackrel{(a)}{\approx} \left(\left[1 - e^{-\frac{P_s}{M-1}} \right]^{-1} - 2 \right) \frac{1}{\log_2 M} \quad (15)$$

$$\stackrel{(b)}{\approx} \left(\frac{M-1}{P_s} - 2 \right) \frac{1}{\log_2 M}, \quad (16)$$

where (a) comes from the approximation $\ln(1 - z) \approx -z$, $|z| \ll 1$, and the fact that P_s scales as $o(1)$. Also, (b) follows from the approximation $e^{-z} = \sum_{n=0}^{\infty} (-1)^n \frac{z^n}{n!} \approx 1 - z$, $|z| \ll 1$. It is concluded from (16) that the first term in (12) is also a monotonically increasing function of M . As a result, the minimum total energy consumption \mathcal{E}_N^{FS} is achieved at $\hat{M} = 2$ for all values of d and η .

M-ary QAM: For M -ary QAM with the square constellation, each $b = \log_2 M$ bits of the message is mapped to the symbol S_i , $i = 0, 1, \dots, M - 1$, with the symbol duration T_s^{QA} . Assuming the raised-cosine filter is used for the pulse shaping, the channel bandwidth of MQAM is given by $B \approx \frac{1}{2T_s^{QA}}$. Thus, using the data rate $R^{QA} = \frac{b}{T_s^{QA}}$, the bandwidth efficiency of MQAM is obtained as $B_{eff}^{QA} \triangleq \frac{R^{QA}}{B} = 2 \log_2 M$ which is a logarithmically increasing function of M . To address the impact of M on the energy efficiency, we derive the active mode duration T_{ac}^{QA} in terms of M as follows:

$$T_{ac}^{QA} = \frac{N}{b} T_s^{QA} = \frac{N}{2B \log_2 M}. \quad (17)$$

It is seen that an increase in M results in a decrease in T_{ac}^{QA} . Also compared to (5) for the NC-MFSK, it is concluded that $T_{ac}^{QA} = \frac{1}{2M} T_{ac}^{FS}$. Interestingly, it seems that the large constellation sizes M would result in the lower energy consumption due to the smaller values of T_{ac}^{QA} . However, as we will show later, the total energy consumption of a MQAM is not necessarily a monotonically decreasing function of M . For this purpose, we obtain the transmit energy consumption $\mathcal{P}_t^{QA} T_{ac}^{QA}$ with a similar argument as for MFSK. It is shown in [16, pp. 226] and [13] that the average SER of a coherent MQAM is upper bounded by

$$P_s = \frac{4(M-1)}{3\bar{\gamma}^{QA} + 2(M-1)} \left(1 - \frac{1}{\sqrt{M}} \right), \quad (18)$$

where $\bar{\gamma}^{QA} = \frac{\Omega}{\mathcal{L}_d} \frac{\mathcal{E}_t^{QA}}{N_0}$ denotes the average received SNR with the energy per symbol \mathcal{E}_t^{QA} . As a result,

$$\mathcal{E}_t^{QA} \triangleq \mathcal{P}_t^{QA} T_s^{QA} = \frac{2(M-1)}{3} \left[2 \left(1 - \frac{1}{\sqrt{M}} \right) \frac{1}{P_s} - 1 \right] \frac{\mathcal{L}_d N_0}{\Omega}. \quad (19)$$

In considering the effect of the DC-DC converter, the output energy consumption of transmitting N -bit during the active mode period is computed as

$$\frac{\mathcal{P}_t^{QA}}{\chi_e} T_{ac}^{QA} = \frac{T_{ac}^{QA}}{T_s^{QA}} \frac{\mathcal{E}_t^{QA}}{\chi_e} = \frac{2(M-1)}{3} \left[2 \left(1 - \frac{1}{\sqrt{M}} \right) \frac{1}{P_s} - 1 \right] \frac{\mathcal{L}_d N_0}{\chi_e \Omega} \frac{N}{\log_2 M}, \quad (20)$$

which is a monotonically increasing function of M for every value of P_s , d and η . For the sensor node with the MQAM modulator,

$$\mathcal{P}_{ct}^{QA} = \mathcal{P}_{DAC}^{QA} + \mathcal{P}_{Sy}^{QA} + \mathcal{P}_{Mix}^{QA} + \mathcal{P}_{Filt}^{QA} + \mathcal{P}_{Amp}^{QA}, \quad (21)$$

where \mathcal{P}_{DAC}^{QA} and \mathcal{P}_{Mix}^{QA} denote the power consumption of DAC and mixer, respectively. It is shown that $\mathcal{P}_{Amp}^{QA} = \alpha^{QA} \mathcal{P}_t^{QA}$, where $\alpha^{QA} = \frac{\xi}{\vartheta} - 1$ with $\xi = 3\frac{\sqrt{M}-1}{\sqrt{M}+1}$ and $\vartheta = 0.35$ [5]. In addition, the circuit power consumption of the sink with the coherent MQAM is obtained as

$$\mathcal{P}_{cr}^{QA} = \mathcal{P}_{LNA}^{QA} + \mathcal{P}_{Mix}^{QA} + \mathcal{P}_{Sy}^{QA} + \mathcal{P}_{Filt}^{QA} + \mathcal{P}_{IFA}^{QA} + \mathcal{P}_{ADC}^{QA}. \quad (22)$$

Also, with a similar argument as for MFSK, we assume that the circuit power consumption during transient mode period T_{tr}^{QA} is governed by the frequency synthesizer. As a result, the total energy consumption of a coherent MQAM for transmitting N -bit in each period T_N is obtained as

$$\begin{aligned} \mathcal{E}_N^{QA} = & (1 + \alpha^{QA}) \frac{2(M-1)}{3} \left[2 \left(1 - \frac{1}{\sqrt{M}} \right) \frac{1}{P_s} - 1 \right] \frac{\mathcal{L}_d N_0}{\chi_e \Omega} \frac{N}{\log_2 M} + \\ & \frac{1}{\chi_e} \left[(\mathcal{P}_c^{QA} - \mathcal{P}_{Amp}^{QA}) \frac{N}{2B \log_2 M} + 2\mathcal{P}_{Sy}^{QA} T_{tr}^{QA} \right]. \end{aligned} \quad (23)$$

Although, there is no constraint on the maximum size M for MQAM, to make a fair comparison to the MFSK scheme, we use the same M_{max} as MFSK. Taking this into account, the optimization problem is to determine the optimum $M \in [4, M_{max}]$ subject to $d > 0$ and $\eta_{min} \leq \eta \leq \eta_{max}$, such that \mathcal{E}_N^{QA} can be minimized.

It is seen that the first term in (23) is a monotonically increasing function of M for every value of P_s , d and η , while the second term is a monotonically decreasing function of M which is independent of d and η . For the above optimization and for a given P_s , we have two following scenarios based on the distance d :

Case 1: For large values of d where the first term in (23) is dominant, the objective function \mathcal{E}_N^{QA} is a monotonically increasing function of M and is minimized at $M = 4$, equivalent to the 4-QAM scheme.

Case 2: Let assume that d is small enough. One possible case may happen is when the total energy consumption \mathcal{E}_N^{QA} for small sizes M is governed by the second term in (23). For this situation, either the

TABLE II
SYSTEM EVALUATION PARAMETERS

$\chi_e = 0.8$	$N_0 = -180$ dBm	$\mathcal{P}_{DAC} = 7$ mw
$B = 62.5$ KHz	$\mathcal{P}_{ED} = 3$ mw	$\mathcal{P}_{ADC} = 7$ mw
$M_l = 40$ dB	$\mathcal{P}_{Sy} = 10$ mw	$\mathcal{P}_{Mix} = 7$ mw
$\mathcal{L}_1 = 30$ dB	$\mathcal{P}_{Filt} = 2.5$ mw	$\mathcal{P}_{LNA} = 9$ mw
$\Omega = 1$	$\mathcal{P}_{Filtr} = 2.5$ mw	$\mathcal{P}_{IFA} = 3$ mw

objective function behaves as a monotonically decreasing function of M for every value of M , or for a large constellation size M , the first term would be dominant, meaning that \mathcal{E}_N^{QA} increases when M grows. In the former scenario, the optimum M is achieved at $\hat{M} = M_{max}$; whereas in the latter scenario, there exists a minimum value for \mathcal{E}_N^{QA} , where the optimum M for this point is obtained by the intersection between the first and second terms, i.e.,

$$(1 + \alpha^{QA}) \frac{2(M-1)}{3} \left[2 \left(1 - \frac{1}{\sqrt{M}} \right) \frac{1}{P_s} - 1 \right] \frac{\mathcal{L}_d N_0}{\chi_e \Omega} \frac{N}{\log_2 M} = \frac{1}{\chi_e} \left[\frac{N(\mathcal{P}_c^{QA} - \mathcal{P}_{Amp}^{QA})}{2B \log_2 M} + 2\mathcal{P}_{Sy}^{QA} T_{tr}^{QA} \right].$$

Since, P_s scales as $o(1)$ and ignoring the term $\mathcal{P}_{Sy}^{QA} T_{tr}^{QA}$ to simplify our analysis, the optimum M which minimizes (23) is obtained by the following equation:

$$M - 1 - \sqrt{M} + \frac{1}{\sqrt{M}} \approx \frac{\phi(d, \eta)}{1 + \alpha^{QA}}, \quad (24)$$

where $\phi(d, \eta) \triangleq \frac{\mathcal{P}_c^{QA} - \mathcal{P}_{Amp}^{QA}}{2B} \frac{3P_s \Omega}{4\mathcal{L}_d N_0}$ and the fact that α^{QA} is a function of M .

To gain more insight to the above optimization problem, we use a specific numerical example with the simulation parameters summarized in Table II³. We assume $P_s = 10^{-3}$, $4 \leq M \leq 64$ and $2.5 \leq \eta \leq 6$. Fig. 2 illustrates the total energy consumption of MQAM versus M for different values of d . It is seen that \mathcal{E}_N^{QA} exhibits different trends depending on the distance d and the path-loss exponent η . For instance, for large values of d and η , \mathcal{E}_N^{QA} is an increasing function of M , where the optimum value of M is achieved at $\hat{M} = 4$ as expected. This is because, in this case, the first term in (23) corresponding to the RF signal energy consumption dominates \mathcal{E}_N^{QA} . Table III details the optimum values of M which minimizes \mathcal{E}_N^{QA} for

³For more details in the simulation parameters, we refer the reader to [13] and its references.

TABLE III

OPTIMUM M IN THE MQAM OPTIMIZATION PROBLEM FOR $P_s = 10^{-3}$ AND DIFFERENT VALUES OF d AND $2.5 \leq \eta \leq 6$

d (m)	$\eta = 2.5$	$\eta = 3$	$\eta = 4$	$\eta = 5$	$\eta = 6$
1	64	64	64	64	64
10	64	64	43	10	4
20	64	50	8	4	4
40	43	13	4	4	4
80	14	5	4	4	4
100	10	4	4	4	4
150	6	4	4	4	4
200	5	4	4	4	4

some values of $1 \leq d \leq 200$ m and $2.5 \leq \eta \leq 6$. We use these results to compare the energy efficiency of the optimized MQAM with the other schemes in the subsequent sections.

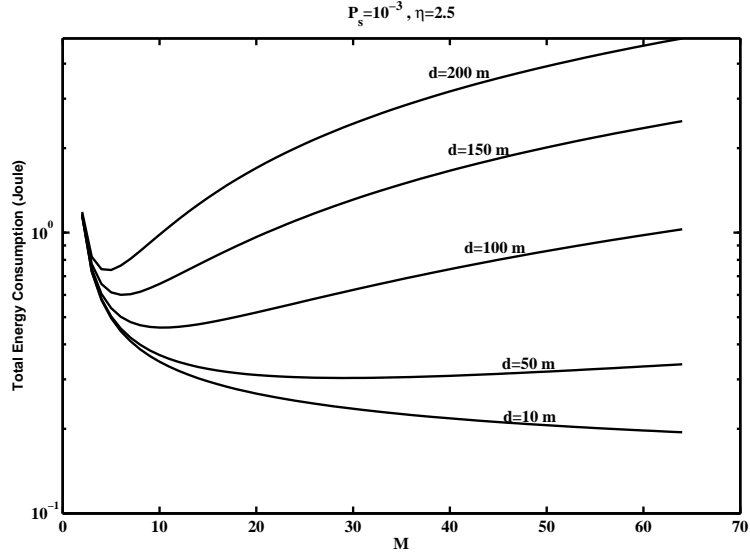
Offset-QPSK: For performance comparison, we choose the conventional OQPSK modulation which is used as a reference in the IEEE 802.15.4/ZigBee protocols. We also follow the same differential OQPSK structure mentioned in [6, p. 50] to eliminate the need for a coherent phase reference at the sink node. For this configuration, the channel bandwidth and the data rate are determined by $B \approx \frac{1}{T_s^{OQ}}$ and $R^{OQ} = \frac{2}{T_s^{OQ}}$, respectively. As a result, the bandwidth efficiency of OQPSK is obtained as $B_{eff}^{OQ} \triangleq \frac{R^{OQ}}{B} = 2$ (b/s/Hz). Since we have 2 bits in each symbol period T_s^{OQ} , it is concluded that

$$T_{ac}^{OQ} = \frac{N}{2} T_s^{OQ} = \frac{N}{2B}. \quad (25)$$

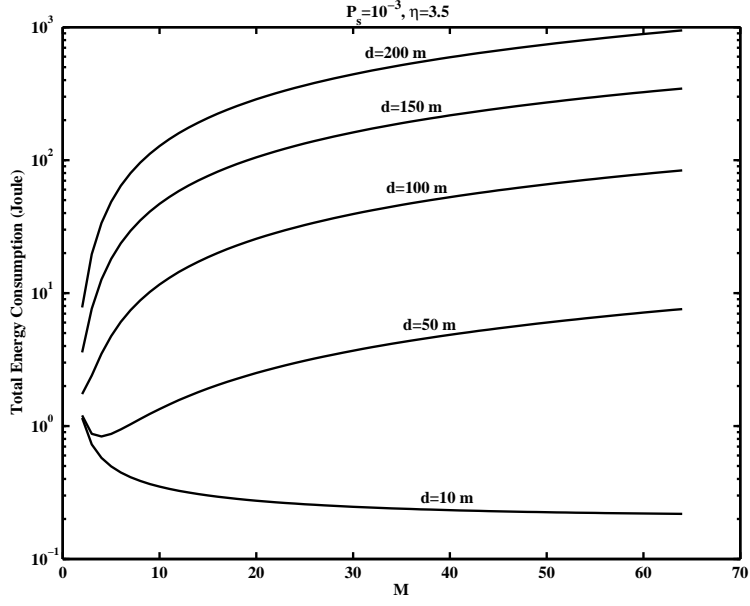
Compared to (5) and (17), we have $T_{ac}^{OQ} = (\log_2 M) T_{ac}^{QA}$ with $M \geq 4$, while for the optimized MFSK, $T_{ac}^{OQ} = \frac{1}{4} T_{ac}^{FS}$. More precisely, it is revealed that $T_{ac}^{QA} < T_{ac}^{OQ} < T_{ac}^{FS}$. To determine the transmit energy consumption of the differential OQPSK scheme, we derive \mathcal{E}_t^{OQ} in terms of the average SER. It is shown in [17] and [13] that the average SER of the differential OQPSK is upper bounded by

$$P_s = \sqrt{\frac{1 + \sqrt{2}}{2}} \frac{4}{(2 - \sqrt{2})\bar{\gamma}^{OQ} + 4}, \quad (26)$$

where $\bar{\gamma}^{OQ} = \frac{\Omega}{\mathcal{L}_d} \frac{\mathcal{E}_t^{OQ}}{N_0}$. With a similar argument as for MFSK and MQAM, the energy consumption of



(a)



(b)

Fig. 2. Total energy consumption \mathcal{E}_N^{QA} vs. M over a Rayleigh fading channel with path-loss for $P_s = 10^{-3}$, a) $\eta = 2.5$, and b) $\eta = 3.5$.

transmitting N -bit during T_{ac}^{OQ} is computed as

$$\frac{\mathcal{P}_t^{OQ}}{\chi_e} T_{ac}^{OQ} = \frac{T_{ac}^{OQ}}{T_s^{OQ}} \frac{\mathcal{E}_t^{OQ}}{\chi_e} = \left[\frac{1}{2 - \sqrt{2}} \left(\frac{4}{P_s} \sqrt{\frac{1 + \sqrt{2}}{2}} - 4 \right) \right] \frac{\mathcal{L}_d N_0 N}{\chi_e \Omega \frac{N}{2}}. \quad (27)$$

In addition, for the sensor node with the OQPSK modulator, $\mathcal{P}_{ct}^{OQ} \approx \mathcal{P}_{DAC}^{OQ} + \mathcal{P}_{Sy}^{OQ} + \mathcal{P}_{Mix}^{OQ} + \mathcal{P}_{Filt}^{OQ} + \mathcal{P}_{Amp}^{OQ}$,

where we assume that the power consumption of the differential encoder is negligible, and $\mathcal{P}_{Amp}^{OQ} = \alpha^{OQ} \mathcal{P}_t^{OQ}$, with $\alpha^{OQ} = 0.33$. In addition, the circuit power consumption of the sink with the differential detection OQPSK is obtained as $\mathcal{P}_{cr}^{OQ} = \mathcal{P}_{LNA}^{OQ} + \mathcal{P}_{Mix}^{OQ} + \mathcal{P}_{Sy}^{OQ} + \mathcal{P}_{Filt}^{OQ} + \mathcal{P}_{IF}^{OQ} + \mathcal{P}_{ADC}^{OQ}$. As a result, the total energy consumption of a differential OQPSK system for transmitting N -bit in each period T_N is obtained as

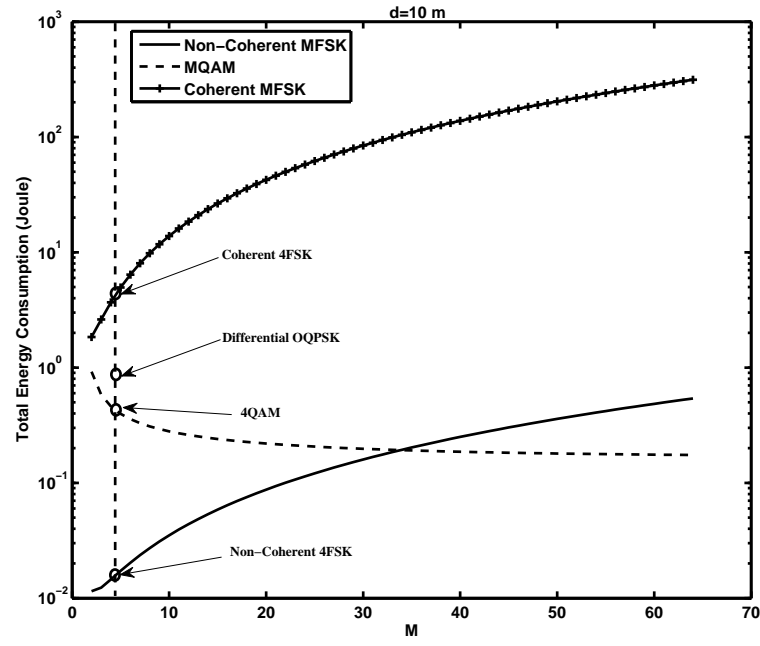
$$\mathcal{E}_N^{OQ} = (1 + \alpha^{OQ}) \left[\frac{1}{2 - \sqrt{2}} \left(\frac{4}{P_s} \sqrt{\frac{1 + \sqrt{2}}{2}} - 4 \right) \right] \frac{\mathcal{L}_d N_0 N}{\chi_e \Omega} \frac{1}{2} + \frac{1}{\chi_e} \left[(\mathcal{P}_c^{OQ} - \mathcal{P}_{Amp}^{OQ}) \frac{N}{2B} + 2\mathcal{P}_{Sy}^{OQ} T_{tr}^{OQ} \right]. \quad (28)$$

IV. NUMERICAL RESULTS

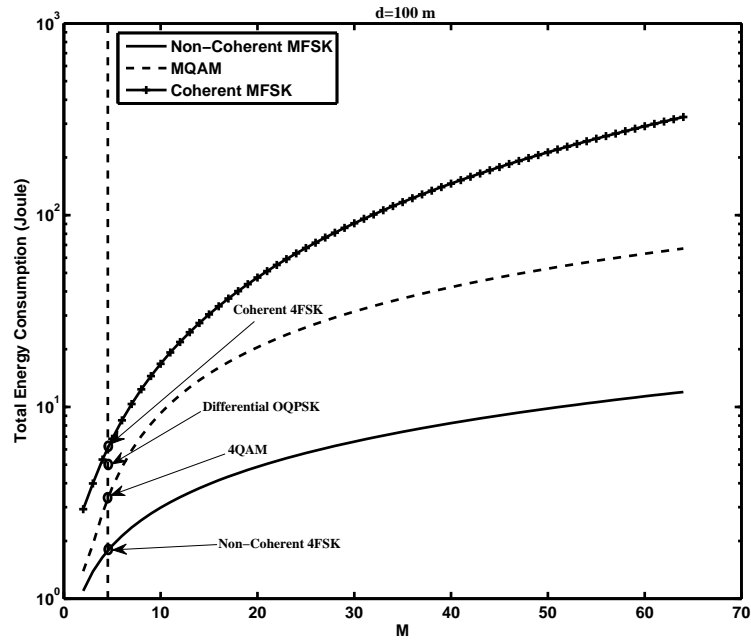
In this section, we present some numerical evaluations using realistic parameters from the IEEE 802.15.4 standard and state-of-the art technology to confirm the energy efficiency analysis discussed in Section III. We assume that all the modulations operate in the carrier frequency $f_0 = 2.4$ GHz Industrial Scientist and Medical (ISM) unlicensed band utilized in the IEEE 802.15.4 standard [6]. According to the FCC 15.247 RSS-210 standard for United States/Canada, the maximum allowed antenna gain is 6 dBi [18]. In this work, we assume that $\mathcal{G}_t = \mathcal{G}_r = 5$ dBi. Thus for the $f_0 = 2.4$ GHz, \mathcal{L}_1 (dB) $\triangleq 10 \log_{10} \left(\frac{(4\pi)^2}{\mathcal{G}_t \mathcal{G}_r \lambda^2} \right) \approx 30$ dB, where $\lambda \triangleq \frac{3 \times 10^8}{f_0} = 0.125$ m. We assume that in each period T_N , the data frame $N = 1024$ bytes (or equivalently $N = 8192$ bits) is generated for transmission for all the modulations, where T_N is assumed to be 1.4 s. The channel bandwidth is set to the $B = 62.5$ KHz, according to the IEEE 802.15.4 standard [6, p. 49]. In addition, we assume that the path-loss exponent is in the range of 2.5 to 6⁴. We use the system parameters summarized in Table II for simulations. It is concluded from $\frac{M_{max}}{\log_2 M_{max}} = \frac{\zeta B}{N} (T_N - T_{tr}^{FS})$ that $M_{max} \approx 64$ (or equivalently $b_{max} \approx 6$) for NC-MFSK. Since, there is no constraint on the maximum M in MQAM, we choose $4 \leq M \leq 64$ for MQAM to be consistent with MFSK.

Fig. 3 compares the energy efficiency of the modulation schemes investigated in Section III versus M for $P_s = 10^{-3}$, $\eta = 3.5$ and different values of d . It is revealed from Fig. 3-a that for $M < 35$, NC-MFSK

⁴ $\eta = 2$ is regarded as a reference state for the propagation in free space and is unattainable in practice. Also, $\eta = 4$ is for relatively lossy environments, and for indoor environments, the path-loss exponent can reach values in the range of 4 to 6.



(a)



(b)

Fig. 3. Total energy consumption of transmitting N -bit vs. M for MFSK, MQAM and differential OQPSK over a Rayleigh fading channel with path-loss and $P_s = 10^{-3}$, a) $d = 10$ m, and b) $d = 100$ m.

TABLE IV
ENERGY-EFFICIENT MODULATION FOR $P_s = 10^{-3}$ AND DIFFERENT VALUES OF d AND η

d (m)	$\eta = 2.5$	$\eta = 3$	$\eta = 4$	$\eta = 5$	$\eta = 6$
1	64QAM	64QAM	64QAM	64QAM	64QAM
10	64QAM	64QAM	NC-BFSK	NC-BFSK	NC-BFSK
20	64QAM	NC-BFSK	NC-BFSK	NC-BFSK	NC-BFSK
40	NC-BFSK	NC-BFSK	NC-BFSK	NC-BFSK	NC-BFSK
80	NC-BFSK	NC-BFSK	NC-BFSK	NC-BFSK	NC-BFSK
100	NC-BFSK	NC-BFSK	NC-BFSK	NC-BFSK	NC-BFSK
150	NC-BFSK	NC-BFSK	NC-BFSK	NC-BFSK	NC-BFSK
200	NC-BFSK	NC-BFSK	NC-BFSK	NC-BFSK	NC-BFSK

is more energy-efficient than MQAM, differential OQPSK and coherent MFSK for $d = 10$ m and $\eta = 3.5$, while when M grows, 64-QAM outperforms the other schemes for $d = 10$ m. The latter result is well supported by the Case 2 in the MQAM optimization discussed in Section III. However, NC-MFSK for a small size M benefits from the advantage of less complexity and cost in implementation than 64-QAM. Furthermore, as shown in Fig. 3-b, the total energy consumption of both MFSK and MQAM for large d increase logarithmically with M which verify the optimization solutions for the NC-MFSK and Case 1 for the MQAM in Section III. Also, it is seen that NC-MFSK exhibits the energy efficiency better than the other schemes when d increases.

The optimized modulations for different transmission distance d and $2.5 \leq \eta \leq 6$ are listed in Table IV. For these results, we use the optimized MQAM detailed in Table III and the fact that for NC-MFSK, $\hat{M} = 2$ is the optimum value which minimizes \mathcal{E}_N^{FS} for every d and η . From Table IV, it is found that although 64-QAM outperforms NC-BFSK for very short range WSNs, it should be noted that using MQAM with a large constellation size M increases the complexity of the system. In particular, when we know that MQAM utilizes the coherent detection at the sink node. In other words, there exists a trade-off between the complexity and the energy efficiency in using MQAM for small values of d .

Up to now, we have investigated the energy efficiency of the sinusoidal carrier-based modulations

TABLE V

TOTAL ENERGY CONSUMPTION (IN JOULE) OF NC-MFSK, MQAM AND OQPSK OVER A RICIAN FADING CHANNEL WITH PATH-LOSS
FOR $P_s = 10^{-3}$ AND $\eta = 3.5$

	$K = 1$ dB				$K = 10$ dB			$K = 15$ dB		
	M	OQPSK	NC-MFSK	MQAM	OQPSK	NC-MFSK	MQAM	OQPSK	NC-MFSK	MQAM
d=10 m	4	1.1241	0.0173	0.5621	1.1241	0.0171	0.5620	1.1241	0.0171	0.5620
	16		0.0769	0.2819		0.0765	0.2810		0.0765	0.2810
	64		0.6558	0.1924		0.6545	0.1874		0.6545	0.1874
d=100 m	4	1.2236	0.5835	0.8873	1.1445	0.0194	0.5652	1.1310	0.0175	0.5627
	16		1.4920	3.2049		0.0785	0.2989		0.0767	0.2843
	64		4.6199	16.1010		0.6570	0.2615		0.6547	0.2002

under the assumption of a Rayleigh fading channel with path-loss. It is also of interest to evaluate the energy efficiency of the aforementioned modulation schemes operating over the more general Rician model which includes the LOS path. For this purpose, let assume that the instantaneous channel coefficient correspond to symbol i is $G_i = \frac{h_i}{\mathcal{L}_d}$, where h_i is assumed to be Rician distributed with pdf $f_{h_i}(r) = \frac{r}{\sigma^2} e^{-\frac{r^2+A^2}{2\sigma^2}} I_0\left(\frac{rA}{\sigma^2}\right)$, $r \geq 0$, where A denotes the peak amplitude of the dominant signal, $2\sigma^2 \triangleq \Omega$ is the average power of non-LOS multipath components [19, p. 78]. For this model, $\mathbb{E}[|h_i|^2] = A^2 + 2\sigma^2 = 2\sigma^2(1 + K)$, where $K(\text{dB}) \triangleq 10 \log \frac{A^2}{2\sigma^2}$ is the Rician factor. The value of K is a measure of the severity of the fading. For instance, $K(\text{dB}) \rightarrow -\infty$ implies Rayleigh fading and $K(\text{dB}) \rightarrow \infty$ represents AWGN channel. Table V summarized the energy efficiency results of the previous modulations over a Rician fading channel with path-loss for $P_s = 10^{-3}$ and $\eta = 3.5$. It is seen from Table V that NC-MFSK with a small size M has less total energy consumption than the other schemes in Rician fading channel with path-loss.

The above results make NC-MFSK with a small M attractive for using in WSNs, since this modulation already has the advantage of less complexity and cost in implementation than MQAM, differential OQPSK and coherent MFSK, and has less total energy consumption. In addition, since for energy-constrained WSNs, data rates are usually low, using M-ary NC-FSK schemes with a small M are desirable. The

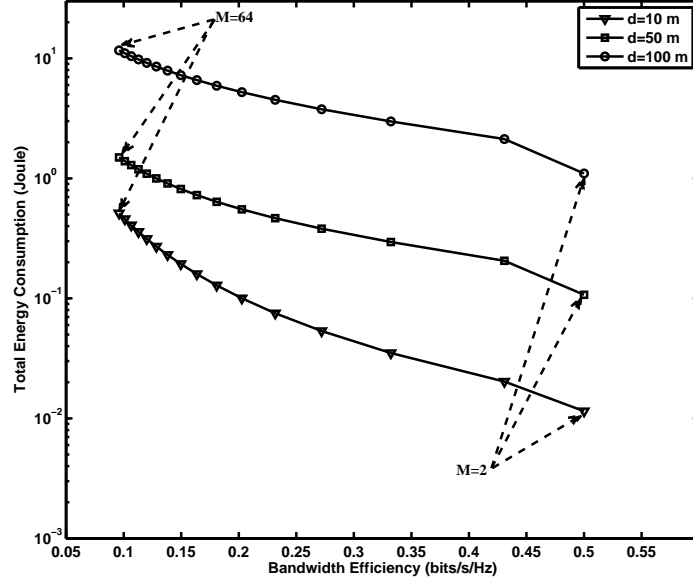


Fig. 4. Total energy consumption of transmitting N -bit versus bandwidth efficiency for NC-MFSK, and for $P_s = 10^{-3}$ and different values of d and M .

sacrifice, however, is the bandwidth efficiency of NC-MFSK (when M increases) which is a critical factor in band-limited WSNs. Since most of WSN applications operate in unlicensed bands where large bandwidth is available, NC-MFSK can surpass the spectrum constraint in WSNs. To have more insight into the above discussions for the NC-MFSK, we plot the total energy consumption of NC-MFSK as a function of B_{eff}^{FS} for different values of M and d in Fig. 4. In all cases, we observe that the minimum \mathcal{E}_N^{FS} is achieved at low values of distance d and for $M = 2$, which corresponds to the maximum bandwidth efficiency $B_{eff}^{FS} = 0.5$.

The analysis and numerical evaluations so far implicitly focused on the sinusoidal carrier-based modulations with the bandwidth $B = 62.5$ KHz. To complete our analysis, it is of interest to compare the energy efficiency of the optimized NC-MFSK with the On-Off Keying (OOK), known as the simplest UWB modulation scheme. For this purpose, we first derive the total energy consumption of OOK with a similar manner as for sinusoidal carrier-based modulations. Then, we evaluate the energy efficiency of OOK in terms of distance d . For simplicity of the notation, we use the superscript ‘OK’ for OOK modulation scheme.

V. ENERGY CONSUMPTION ANALYSIS OF OOK

For OOK, the number of bits per symbol is defined as $b = \log_2 M = 1$. An OOK transmitted signal corresponding to the symbol $a_i \in \mathbb{M}_N$ is given by $x_i^{OK}(t) = \sqrt{\mathcal{E}_t^{OK}} a_i p(t - iT_s^{OK})$, where $p(t)$ is an ultra-short pulse of width T_p with unit energy, \mathcal{E}_t^{OK} is the transmit energy consumption per symbol, and T_s^{OK} is the OOK symbol duration. The ratio $\frac{T_p}{T_s^{OK}}$ is defined as the *duty-cycle factor* of an OOK signal, which is the fractional on-time of the OOK “1” pulse. The channel bandwidth and the data rate of an OOK are determined as $B \approx \frac{1}{T_p}$ and $R^{OK} = \frac{1}{T_s^{OK}}$, respectively. As a result, the bandwidth efficiency of an OOK is obtained as $B_{eff}^{OK} \triangleq \frac{R^{OK}}{B} = \frac{T_p}{T_s^{OK}} \leq 1$ (b/s/Hz) which controls by the duty-cycle factor. Note that during the transmission of the OOK “0” pulse, the filter and the power amplifier of the OOK modulator are powered off. During this time, however, the receiver is turned on to detect zero pulses. For this reason, we still use the same definition for active mode period T_{ac}^{OK} as used for the sinusoidal carrier-based modulations as follows:

$$T_{ac}^{OK} = \frac{N}{b} T_s^{OK} = N T_s^{OK}. \quad (29)$$

Depend upon the duty-cycle factor, T_{ac}^{OK} can be expressed in terms of bandwidth B . For instance, for an OOK with the duty-cycle factor $\frac{T_p}{T_s^{OK}} = \frac{1}{2}$, we have $T_{ac}^{OK} = 2NT_p = \frac{2N}{B}$, and $B_{eff}^{OK} = \frac{1}{2}$. Compared to (4) for the NC-MFSK, it is concluded that B_{eff}^{OK} with the duty-cycle factor $\frac{T_p}{T_s^{OK}} = \frac{1}{2}$ is the same as that of the optimized MFSK (i.e., $\hat{M} = 2$) in Section III. It is shown in [20, pp. 490-504] that the average SER of an OOK with non-coherent detection is upper bounded by

$$P_s = \frac{1}{\bar{\gamma}^{OK} + 2}, \quad (30)$$

where $\bar{\gamma}^{OK} = \frac{\Omega}{\mathcal{L}_d} \frac{\mathcal{E}_t^{OK}}{N_0}$ denotes the average received SNR. Thus, the transmit energy consumption per symbol is obtained as $\mathcal{E}_t^{OK} \triangleq \mathcal{P}_t^{OK} T_p = \left(\frac{1}{P_s} - 2 \right) \frac{\mathcal{L}_d N_0}{\Omega}$ which corresponds to transmitting “1” pulse. An interesting point is that \mathcal{E}_t^{OK} scales the same as \mathcal{E}_t^{FS} obtained in (8) for NC-BFSK. This can be easily proved by using the approximation method in (14)-(16). It should be noted that the energy consumption of transmitting N -bit during the active mode period, denoted by $\frac{\mathcal{P}_t^{OK}}{\chi_e} T_{ac}^{OK}$, is equivalent to the energy consumption of transmitting L -bit “1” in \mathbb{M}_N , where L is a binomial random variable with parameters

TABLE VI
OOK SYSTEM EVALUATION PARAMETERS

$N = 20000$	$N_0 = -180$ dB	$\mathcal{P}_{PG} = 675$ μ W
$B = 500$ MHz	$T_N = 100$ msec	$\mathcal{P}_{LNA} = 3.1$ mW
$M_l = 40$ dB	$T_{tr} = 2$ nsec	$\mathcal{P}_{ED} = 3$ mW
$\mathcal{L}_1 = 30$ dB	$\mathcal{P}_{Filt} = 2.5$ mW	$\mathcal{P}_{ADC} = 7$ mW
$\chi_e = 0.8$	$\mathcal{P}_{Filt_r} = 2.5$ mW	$\mathcal{P}_{Int} = 3$ mW

(N, q) . Assuming uncorrelated and equally likely binary data a_i , we have $q = \frac{1}{2}$. Hence, $\frac{\mathcal{P}_t^{OK}}{\chi_e} T_{ac}^{OK} = \frac{L}{\chi_e} \mathcal{E}_t^{OK} = L \left(\frac{1}{P_s} - 2 \right) \frac{\mathcal{L}_d N_0}{\chi_e \Omega}$, where L has the probability mass function $\Pr\{L = \ell\} = \binom{N}{\ell} \left(\frac{1}{2}\right)^N$ with $\mathbb{E}[L] = \frac{N}{2}$.

We denote the power consumption of pulse generator, power amplifier and filter as \mathcal{P}_{PG}^{OK} , \mathcal{P}_{Amp}^{OK} and \mathcal{P}_{Filt}^{OK} , respectively. Hence, the circuit energy consumption of the sensor node during T_{ac}^{OK} is represented as a function of the random variable L as $\mathcal{P}_{ct}^{OK} T_{ac}^{OK} = \mathcal{P}_{PG}^{OK} T_{ac}^{OK} + LT_p (\mathcal{P}_{Filt}^{OK} + \mathcal{P}_{Amp}^{OK})$, where the factor LT_p comes from the fact that the filter and the power amplifier are active only during the transmission of L -bit “1”. We assume that $\mathcal{P}_{Amp}^{OK} = \alpha^{OK} \mathcal{P}_t^{OK}$ with $\alpha^{OK} = 0.33$. In addition, the circuit energy consumption of the sink node with a non-coherent detection during T_{ac}^{OK} is obtained as $\mathcal{P}_{cr}^{OK} T_{ac}^{OK} = (\mathcal{P}_{LNA}^{OK} + \mathcal{P}_{ED}^{OK} + \mathcal{P}_{Filt_r}^{OK} + \mathcal{P}_{Int}^{OK} + \mathcal{P}_{ADC}^{OK}) T_{ac}^{OK}$, where \mathcal{P}_{Int}^{OK} is the power consumption of the integrator. With a similar argument as for the sinusoidal carrier-based modulations, we assume that the circuit power consumption during T_{tr}^{OK} is governed by the pulse generator. As a result, the total energy consumption of a non-coherent OOK for transmitting N -bit is obtained as a function of the random variable L as follows:

$$\mathcal{E}_N^{OK}(L) = (1 + \alpha^{OK})L \left(\frac{1}{P_s} - 2 \right) \frac{\mathcal{L}_d N_0}{\chi_e \Omega} + \frac{1}{\chi_e} \left[(\mathcal{P}_{cr}^{OK} + \mathcal{P}_{PG}^{OK}) \frac{2N}{B} + \frac{L}{B} \mathcal{P}_{Filt}^{OK} + 2\mathcal{P}_{PG}^{OK} T_{tr}^{OK} \right], \quad (31)$$

where we use $T_{ac}^{OK} = \frac{2N}{B}$. Since $\mathbb{E}[L] = \frac{N}{2}$, the average $\mathcal{E}_N^{OK}(L)$ is computed as

$$\begin{aligned} \mathcal{E}_N^{OK} &\triangleq \mathbb{E}[\mathcal{E}_N^{OK}(L)] = (1 + \alpha^{OK}) \left(\frac{1}{P_s} - 2 \right) \frac{\mathcal{L}_d N_0}{\chi_e \Omega} \frac{N}{2} + \\ &\quad \frac{1}{\chi_e} \left[(\mathcal{P}_{cr}^{OK} + \mathcal{P}_{PG}^{OK}) \frac{2N}{B} + \frac{N}{2B} \mathcal{P}_{Filt}^{OK} + 2\mathcal{P}_{PG}^{OK} T_{tr}^{OK} \right]. \end{aligned} \quad (32)$$

It should be noted that the OOK scheme uses the channel bandwidth much wider than that of the

sinusoidal carrier-based modulations. Thus, to make a fair comparison with the optimized NC-MFSK, it is reasonable to use the total energy consumption per information bit defined as $\mathcal{E}_b \triangleq \frac{\mathcal{E}_N}{N}$, instead of using \mathcal{E}_N . In our comparison, we use the simulation parameters shown in Table VI [13]. Fig. 5 compares the total energy consumption per information bit of the OOK with that of the optimized NC-MFSK versus communication range d for $P_s = 10^{-3}$ and different values of η . We observe that a significant energy saving is achieved using OOK as compared to the optimized NC-MFSK, when d and η decrease. While, for the indoor environments where η is large, the performance difference between OOK and the optimized NC-MFSK vanishes as d increases. This is because, *i*) the transmission energy consumption in the active mode period is dominant when d increases, *ii*) \mathcal{E}_t^{OK} scales the same as \mathcal{E}_t^{FS} obtained in (8) using (16). Since, UWB modulation schemes use the channel bandwidth much wider than that of the sinusoidal carrier-based modulations, the optimized NC-MFSK is desirable in use for the band-limited and sparse WSNs where the path-loss exponent is large.

VI. CONCLUSION

In this paper, we have analyzed the energy efficiency of some popular modulation schemes to find the distance-based green modulations in a WSN over Rayleigh and Rician flat-fading channels with path-loss. It was demonstrated that among various sinusoidal carrier-based modulations, the optimized NC-MFSK is the most energy-efficient scheme in sparse WSNs for each value of the path-loss exponent, where the optimization is performed over the modulation parameters. In addition, NC-MFSK with a small M is attractive for using in WSNs, since this modulation already has the advantage of less complexity and cost in implementation than MQAM, differential OQPSK and coherent MFSK, and has less total energy consumption. Furthermore, MFSK has a faster start-up time than other schemes. Moreover, since for energy-constrained WSNs, data rates are usually low, using M-ary NC-FSK schemes with a small M are desirable. The sacrifice, however, is the bandwidth efficiency of NC-MFSK when M increases. Since most of WSN applications requires low to moderate bandwidth, a loss in the bandwidth efficiency can be tolerable, in particular for the unlicensed band applications where large bandwidth is available. It also

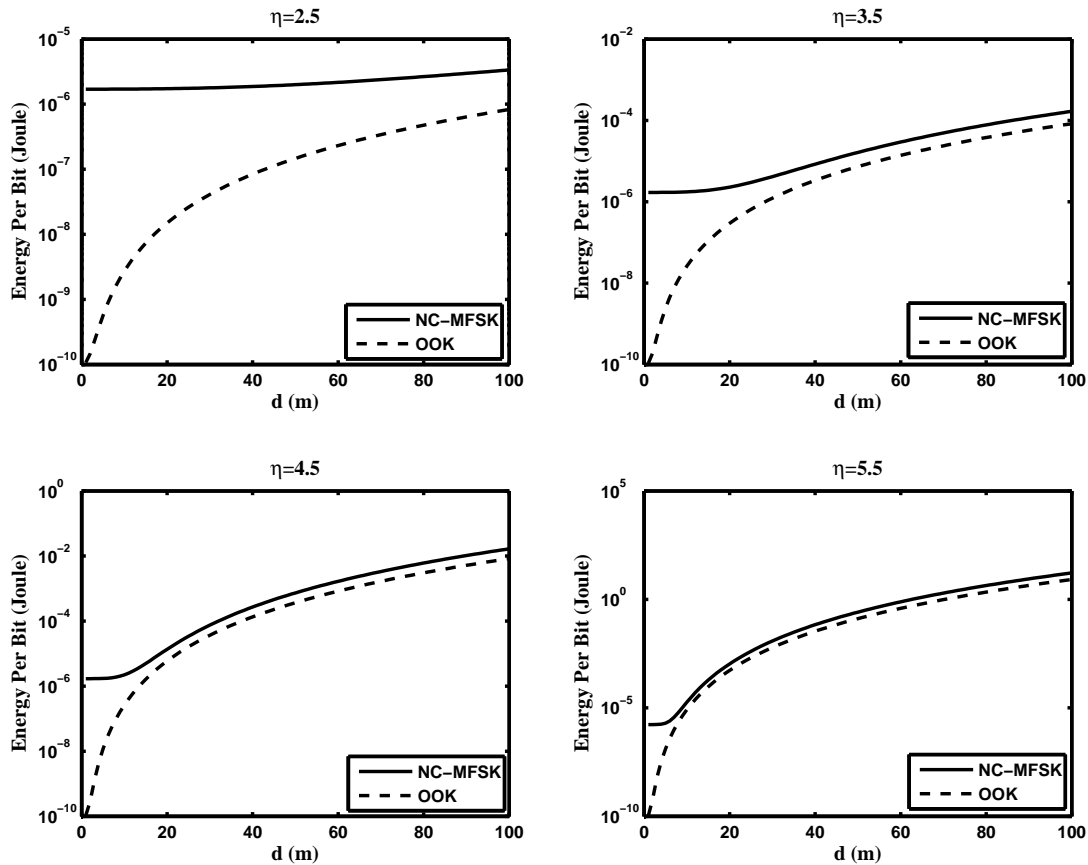


Fig. 5. Total energy consumption per information bit versus d for OOK and the optimized NC-MFSK, and for $P_s = 10^{-3}$.

found that OOK has a significant energy saving as compared to the optimized NC-MFSK in dense WSNs with small values of path-loss exponent. While, for the indoor environments where the path-loss exponent is large, the performance difference between OOK and the optimized NC-MFSK vanishes as the distance between the sensor and sink nodes increases. In this case, the optimized NC-MFSK is attractive in use for the band-limited and sparse indoor WSNs.

REFERENCES

- [1] Abouei, J., Plataniotis, K. N., and Pasupathy, S.: 'Green modulation in dense wireless sensor networks,' *Proc. of IEEE International Conference on Acoustics, Speech and Signal Processing (ICASSP'10)*, Dallas, Texas, USA, March 2010, pp. 3382–3385.
- [2] Abouei, J., Brown, J. D., Plataniotis, K. N., and Pasupathy, S.: 'On the energy efficiency of LT codes in proactive wireless sensor networks,' *Proc. of IEEE Biennial Symposium on Communications (QBSC'10)*, Queen's University, Kingston, Canada, May 2010, pp. 114–117.

- [3] Qu, F., Duan, D., Yang, L., and Swami, A.: 'Signaling with imperfect channel state information: A battery power efficiency comparison,' *IEEE Trans. on Signal Processing*, vol. 56, no. 9, Sep. 2008, pp. 4486–4495.
- [4] Garzs, J. E., Calzn, C. B., and Armada, A. G.: 'An energy-efficient adaptive modulation suitable for wireless sensor networks with SER and throughput constraints,' *EURASIP Journal on Wireless Communications and Networking*, vol. 2007, no. 1, Jan. 2007.
- [5] Cui, S., Goldsmith, A. J., and Bahai, A.: 'Energy-constrained modulation optimization,' *IEEE Trans. on Wireless Commun.*, vol. 4, no. 5, Sept. 2005, pp. 2349–2360.
- [6] IEEE Standards, 'Part 15.4: Wireless Medium Access control (MAC) and Physical Layer (PHY) Specifications for Low-Rate Wireless Personal Area Networks (WPANs),' in *IEEE 802.15.4 Standards*, Sept. 2006.
- [7] Mingoo, S., Hanson, S., Sylvester, D., and Blaauw, D., 'Analysis and optimization of sleep modes in subthreshold circuit design,' in *Proc. 44th ACM/IEEE Design Automation Conference*, San Diego, California, June 2007, pp. 694–699.
- [8] Karl, H., and Willig, A.: *Protocols and Architectures for Wireless Sensor Networks*, John Wiley and Sons Inc., first edition, 2005.
- [9] Tanchotikul, S., Supanakoon, P., Promwong, S., and Takada, J.: 'Statistical model RMS delay spread in UWB ground reflection channel based on peak power loss,' in *Proc. of ISCIT'06*, 2006, pp. 619–622.
- [10] Proakis, J. G.: *Digital Communications*, New York: McGraw-Hill, forth edition, 2001.
- [11] Hind Chebbo *et al.*, 'Proposal for Partial PHY and MAC including Emergency Management in IEEE802.15.6,' May 2009, available at IEEE 802.15 WPAN TG6 in Body Area Network (BAN), <http://www.ieee802.org/15/pub/TG6.html>.
- [12] Xiong, F.: *Digital Modulation Techniques*, Artech House, Inc., second edition, 2006.
- [13] Abouei, J., Plataniotis, K. N., and Pasupathy, S.: 'Green modulation in proactive wireless sensor networks,' Technical report, University of Toronto, ECE Dept., Sept. 2009, available at <http://www.dsp.utoronto.ca/~abouei/>.
- [14] Tang, Q., Yang, L., Giannakis, G. B., and Qin, T.: 'Battery power efficiency of PPM and FSK in wireless sensor networks,' *IEEE Trans. on Wireless Commun.*, vol. 6, no. 4, April 2007, pp. 1308–1319.
- [15] Ziemer, R. E., and Peterson, R. L.: *Digital Communications and Spread Spectrum Systems*, New York: Macmillman, 1985.
- [16] Simon, M. K., and Alouini, M.-S.: *Digital Communication over Fading Channels*, New York: Wiley Interscience, second edition, 2005.
- [17] Simon, M.-S.: 'Multiple-bit differential detection of offset QPSK,' *IEEE Trans. on Commun.*, vol. 51, pp. 1004–1011, June 2003.
- [18] 'Range extension for IEEE 802.15.4 and ZigBee applications,' *FreeScale Semiconductor, Application Note*, Feb. 2007.
- [19] Goldsmith, A.: *Wireless Communications*, Cambridge University Press, first edition, 2005.
- [20] Couch, L. W.: *Digital and Analog Communication Systems*, Prentice-Hall, sixth edition, 2001.